

Spatiotemporal Predictive Pre-training for Robotic Motor Control

Jiange Yang^{1†} Bei Liu² Jianlong Fu² Bocheng Pan³

Gangshan Wu¹ Limin Wang^{1‡}

¹ State Key Laboratory for Novel Software Technology, Nanjing University, China

² Microsoft Research

³ Institute of Microelectronics of the Chinese Academy of Sciences

jiangeyang.jgy@gmail.com {Bei.Liu,jianf}@microsoft.com

panbocheng@ime.ac.cn {gswu,lmwang}@nju.edu.cn

Abstract. Robotic motor control necessitates the ability to predict the dynamics of environments and interaction objects. However, advanced self-supervised pre-trained visual representations (PVRs) in robotic motor control, leveraging large-scale egocentric videos, often focus solely on learning the static content features of sampled image frames. This neglects the crucial temporal motion clues in human video data, which implicitly contain key knowledge about sequential interacting and manipulating with the environments and objects. In this paper, we present a simple yet effective robotic motor control visual pre-training framework that jointly performs spatiotemporal predictive learning utilizing large-scale video data, termed as **STP**. Our STP samples paired frames from video clips. It adheres to two key designs in a multi-task learning manner. First, we perform spatial prediction on the masked current frame for learning content features. Second, we utilize the future frame with an extremely high masking ratio as a condition, based on the masked current frame, to conduct temporal prediction of future frame for capturing motion features. These efficient designs ensure that our representation focusing on motion information while capturing spatial details. We carry out the largest-scale evaluation of PVRs for robotic motor control to date, which encompasses 21 tasks within a real-world Franka robot arm and 5 simulated environments. Extensive experiments demonstrate the effectiveness of STP as well as unleash its generality and data efficiency by further post-pre-training and hybrid pre-training.

Keywords: Self-supervised pre-training · Robotic control · Behavior cloning

1 Introduction

In natural language processing and computer vision, the paradigm of adapting pre-trained foundation models from large-scale data to various downstream

[†] This work was performed when Jiange Yang and Bocheng Pan were visiting Microsoft Research as research interns.

[‡] Corresponding author.

tasks has become achieved great success. For example, pre-trained visual representations using self-supervised [38,15,67,2,93] or weakly-supervised [71,25,55] methods exhibit strong generalization ability for visual understanding. However, in robot learning, due to the scarcity and homogeneity of robot data, some groundbreaking methods [53,1] resort to training from scratch only using domain-specific data. Recently, inspired by the success of transfer learning in computer vision, many works [69,73,65,58,59,19] have explored developing a pre-trained visual representation (PVR) using large-scale out-of-domain data for various robotic motor control tasks. Currently, one successful paradigm [73,99,59,19] is to use large-scale ego-centric video datasets [29] and train vanilla vision transformers (ViT) [22] based on MAE [38], which exhibits excellent learning efficiency and generalization ability for learning policy from raw pixel. Among them, the Ego4D [29] dataset offers numerous first-person human-object interaction scenes and good motion clues. We argue that although learning static spatial structure priors from task-relevant pre-training data sources is crucial, designing a more relevant self-supervised proxy task for motor control should not be overlooked. Therefore, in this paper, we aim to develop a more relevant self-supervised proxy task for robotic motor control based on scalable ViT [22] and egocentric videos.

Robotic motor control typically requires fine-grained spatial localization and relatively dense semantics. With its ability to effectively capture low-level geometry and space structure, MAE [38] pre-training excels at this task. However, is dense spatial content sufficient for robotic motor control? Some neuroscientific studies [50,21,88] suggest the brain’s different areas or cells show specialization. Some are dedicated to processing the information of temporal object motion, while others focus on static spatial details. Their combination results in subjective pattern perception. Inspired by this finding, we hypothesize that an effective robotic motor control pre-training proxy task should require joint learning of spatial content features and temporal motion features. However, current methods [73,59,19] use MAE pre-training with image frames from human videos, capturing only static content features. They overlook the temporal motion clues in human videos, which implicitly contain key knowledge about sequential interaction with environment and manipulation of objects. Therefore, we aim to bridge this gap by incorporating these motion clues into our proxy task.

Based on the analysis above, the most critical challenge is the absence of action annotations in human video data for modeling motion. To model interaction and manipulation actions from actionless video data, we propose to implicitly capture them by predicting future frame pixels based on current frame. However, predicting the future frame without any conditions could contain high uncertainty and be extremely difficult. Therefore, we propose to use the future frame with an extremely high masking ratio as a prompt condition, specifically 95%, which serves to reveal some behavior and dynamic priors, i.e. what to do and how to do it. In the experiments section, we will further explore different condition alternatives, including language narration and their combination. Additionally, directly and simply executing temporal prediction could lead the model to overlook static spatial details, and it is also not efficient enough. Therefore, another

technical contribution of STP is to jointly perform spatial prediction by masking the current frame with 75% masking ratio. In summary, we present **STP**, a multi-task self-supervised pre-training framework through spatiotemporal predictive learning. Our STP asymmetrically mask the current frame and future frame from a video clip, using a spatial decoder to conduct spatial prediction for content learning and a temporal decoder to conduct temporal prediction for motion learning. These efficient designs ensure that our pre-trained encoder focusing on motion information while capturing spatial details.

Subsequently, we establish our evaluation scheme. Currently, how to adapt pre-trained visual representations for robotic motor control still remain an open question. Transfer methods include linear probing [69,65,46,59] and fine-tuning [19], while policy learning methods encompass state representation for reinforcement learning [99] and few-shot behavior cloning [69,65,59]. Considering the expensive cost of robot data collection or exploration, we employ a data-efficient paradigm of few-shot behavior cloning by learning from demonstrations (Lfd). To demonstrate the generalization ability of visual representation, our primary evaluation scheme involves freezing the visual encoder when training the policy model. Additionally, considering that fine-tuning ViT with few demonstrations might lead to overfitting and masked modeling exhibits excellent data efficiency [86,102,52] in domain-specific data, we further follow the post-pre-training [7,93,59] paradigm to perform STP pre-training with task-specific data to achieve better results. It is noteworthy that different tasks do not share representation in this setting. Finally, we conduct the largest-scale evaluation of PVRs for robotic motor control to date to demonstrate the effectiveness of STP, which encompasses 21 tasks (2 real-world Franka robot tasks and 19 simulation tasks across 5 environments). The simulation tasks are derived from the union of manipulation and locomotion tasks from prior works [65,59]. In summary, our main contribution is threefold:

- We present STP, a self-supervised visual pre-training framework for robotic motor control, which jointly conducts spatiotemporal prediction for content and motion features learning in a multi-task learning manner.
- From the perspective of pre-training data, we further expand STP by performing hybrid pre-training with more diverse ImageNet-MAE and post-pre-training with task-specific data, unleashing its generality and data efficiency.
- To our best knowledge, we conduct the largest-scale evaluation of PVRs for robotic motor control to date to demonstrate the effectiveness of STP.

2 Related Work

2.1 Pre-trained Visual Representation Learning

Large-scale visual representation pre-training are continually empowering computer vision. The primary supervised learning methods include learning image recognition [40,87] from ImageNet [20] and learning multi-modal alignment [71] from image-text pairs. Currently, self-supervised learning methods are enjoying significant popularity, primarily falling into two main categories. The first

category utilizes contrastive learning [39,15,14] technique or joint-embedding architecture [13] to learn view-invariance. The second category performs masked modeling [7,38,100,95,4,2] and predict the pixel or representation of invisible parts in space. In addition, some methods [106,67,8] have also proposed to combine different optimization objectives in a multi-task learning manner.

Recently pre-trained visual representation learning for robotic motor control have been rapidly developing [69,65,73,99,58,57,46,59,19]. These methods cover different backbones (ResNet [40], ViT [22]), different policy learning methods (reinforcement learning, behavior cloning, reward function and task specification [42]), different adaptation schemes (linear probing, fine-tuning and designing adapters [78,56]), and different evaluation environments (diverse simulation benchmarks). At present, it is still unclear how these factors collectively influence the performance. In this paper, we choose scalable vanilla vision transformer [22] as our backbone and data-efficient few-shot behavior cloning paradigm to conduct policy learning, while ensuring the backbone is frozen during policy training.

2.2 Temporal Predictive Learning

Early works once explored representation learning through future prediction, encompassing image [61], video [35,80] and audio [66]. VideoMAE [86,93] extend MAE [38] to 3D video architecture. Recently TrackMAE [17] and SiamMAE [33] predict the masked future frame based on unmasked current frame, leading to a better capture of temporal correspondence and achieving outstanding performance in object tracking and segmentation tasks. In robot learning, predicting future visual states primarily serves as a transition dynamic model such as World Models [62,77] and Dreamer [76]. [85,9] predict the future visual states using goal image in robot data. GR-1 [97] conducts language-conditioned video prediction for policy model pre-training in a frozen visual representation space. [96] proposed dynamics-aware representation learning, and [82,72] employed forward dynamics for self-supervised pre-training. Some works explored to train video prediction models and utilize visual foresight [32], inverse dynamics models [18], goal-conditioned policy learning [23], and geometry estimation [51] methods for motor control, respectively. [92] fine-tuned pre-trained representations into dynamic and functional distance modules for manipulation tasks. Unlike these works, we utilize the public large-scale egocentric video data and employ masked spatiotemporal predictive learning as a PVR proxy task, instead of designing elaborate architectures or methods for specific predictive tasks [28,37].

2.3 Vision-based Robot Learning

Vision-based robot learning plays a crucial role in robotics community. Recently some related works focus on studying model architectures [44,12,47], observation spaces [107], downstream policy learning methods [41], sim-to-real transfer [79], designing adapters [78,56], learning-from-scratch baseline [36], and affordance model [6,105,45,60], in visuo-motor representation learning. Other related works [70,5,91,101,48] attempt to learn manipulation skills from small-

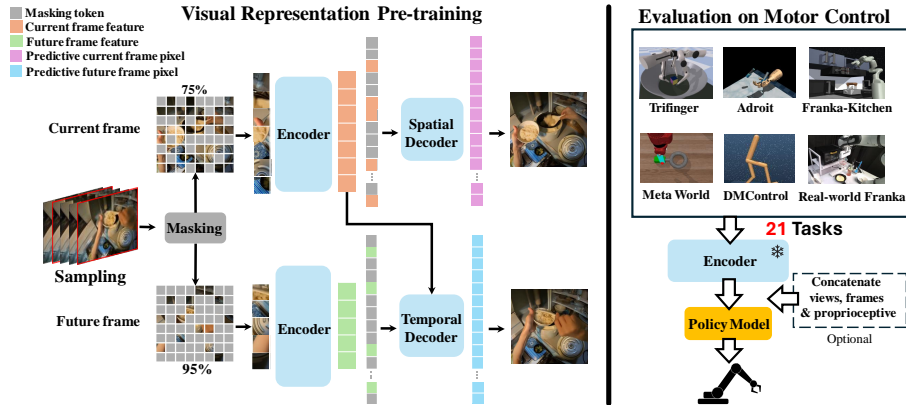


Fig. 1: **Our STP framework.** **Left:** During pre-training, we sample the current frame and the future frame from the video clip, and carry out spatiotemporal predictive pre-training. **Right:** During downstream evaluation, we freeze the pre-trained encoder to extract visual state representations and discard the decoders.

scale and in-domain human videos. In addition, language-conditioned vision robot learning has received significant attention. Some works scale multimodal robotic data [42, 11, 34, 90, 24, 68, 84] or introduce Internet data and knowledge [81, 103, 10, 54, 43, 94, 64] for end-to-end robot learning. In our study, we pre-train a off-the-shelf visual representation from large-scale egocentric video datasets for robotic motor control tasks. Our method is more simple and general for different downstream tasks of motor control.

3 Method

In this section, we describe our method in details. First, we give an overview of our spatiotemporal predictive pretraining (STP) framework. Then, we give a technical description on our core components during pre-training: the masked image encoder and dual decoders scheme. Finally, we describe how to adapt our pre-trained encoder to downstream robotic motor control tasks.

3.1 Overview of STP

As illustrated in Figure 1, our STP aims to pre-train an image encoder for robotic motor control from video datasets. This pre-trained image encoder is subsequently frozen and directly transferred to solve motor control tasks. Specifically, given a video dataset \mathcal{D} , our goal is to learn an image encoder Φ_{enc} , that maps images to the visual representations. During pre-training and post-pre-training, \mathcal{D} represents large-scale out-of-domain videos and task-specific demonstration videos, respectively. After pre-training, we reuse Φ_{enc} for downstream motor control policy learning. Specifically, the downstream task will require an agent

to make sequential action decisions based on visual observations \mathcal{O} . Instead of using the raw observation images as direct input like end-to-end policy learning from pixel, the agent will employ the pre-trained Φ_{enc} to extract its visual state representation $\Phi_{enc}(\mathcal{O})$ for the subsequent policy learning module.

3.2 Masked Image Encoder

We first introduce the pipeline of our image encoder. Our image encoder processes image frames using a vanilla vision transformer [22]. Given a image $\mathbf{I} \in \mathbb{R}^{C \times H \times W}$, we initially process it by the patch embedding layer to obtain its token sequences \mathbf{T} , where $\mathbf{T} = \{P_i\}_{i=1}^N$ and N is the total token number, (e.g., $N = 196$ for a 224×224 image with a patch size of 16×16). Then we add the fixed 2D sine-cosine positional embeddings for all tokens. Following this, we mask and remove a part of tokens, according to a randomly generated masking map $\mathbb{M}(\rho)$, where ρ is the masking ratio. The encoder applies several blocks (consisting of a global self-attention layer and a FFN layer) on all unmasked tokens: $\mathbf{Z} = \Phi_{enc}(\mathbf{T}^u)$, where $\mathbf{T}^u = \{T_i\}_{i \in (1-\mathbb{M}(\rho))}$. During this process, a [CLS] token is added at the beginning.

Then we describe our encoding process during pre-training. We randomly sample two frames from a video clip based on an interval: the current frame \mathbf{I}_c and the future frame \mathbf{I}_f . Following the above pipeline, we randomly generate two asymmetric masking maps for the current frame and the future frame, denoted as $\mathbb{M}_c = \mathcal{M}_c(\rho^c)$ and $\mathbb{M}_f = \mathcal{M}_f(\rho^f)$, respectively. Each of these maps has a different masking ratio. We then use these maps to separately process the two frames and obtain their features, \mathbf{Z}_c and \mathbf{Z}_f . As analyzed above, our STP aims to jointly learn content and motion features by spatiotemporal predictive learning. For content feature learning, we follow MAE [38], masking a portion of the current frame based on \mathbb{M}_c , with $\rho^c = 75\%$, and predict the masked parts during the decoding process. This encourages the model to learn spatial and geometric structure priors from the current frame data through spatial reasoning. For motion feature learning, we establish an objective to predict the future frame based on the masked current frame. However, predicting the future frame without any conditions could be meaningless and extremely challenging. Therefore, we use the future frame with an extremely high masking ratio as a condition, specifically $\rho^f = 95\%$, which reveals some behavior and dynamic priors. In the experiments section, we will further discuss different condition schemes, including language narration and the combination between them. In summary, our encoding process during pre-training can be formally described as follows:

$$\begin{cases} \mathbf{Z}_c = \Phi_{enc}(\mathbf{I}_c, \mathbb{M}_c), \\ \mathbf{Z}_f = \Phi_{enc}(\mathbf{I}_f, \mathbb{M}_f). \end{cases} \quad (1)$$

3.3 Dual Decoders

To jointly capture content and motion features for better spatiotemporal understanding, our STP present a dual decoders scheme to predict both the pixel

of current and future frame simultaneously in a multi-task learning manner. As shown in Figure 1, our dual decoder scheme includes a spatial decoder Φ_{dec_s} for spatial prediction and a temporal decoder Φ_{dec_t} for temporal prediction. We firstly give a technical description on them, respectively. Then we describe how we combine them into our final method.

Spatial Decoder. To capture static content features, our spatial decoder is solely utilized for processing the current frame visual feature. Specifically, after obtaining the masked current frame visual feature \mathbf{Z}_c , we concatenate it with some learnable masking tokens, leading to the formation of $\mathbf{Z}_c^d = \mathbf{Z}_c \cup \{\mathbf{M}_i\}_{i \in \mathbb{M}_c}$, where \mathbb{M}_c is the current frame masking map. Then, each of these tokens further adds a corresponding positional embedding. Subsequently, \mathbf{Z}_c^d undergoes decoding in the decoder and is continuously updated. The architecture of the spatial decoder block aligns with the standard vision encoder block, comprised of a global self-attention layer and a FFN layer. Finally, with the decoded token sequence \mathbf{Z}_c^d , our spatial decoder predicts the invisible tokens of the current frame $\hat{\mathbf{I}}_c^d$, operating under the current frame masking map \mathbb{M}_c .

Temporal Decoder. To capture motion features, our temporal decoder jointly processes the current frame and the future frame which serves as the temporal prediction condition. To elaborate, we firstly obtain the masked current frame visual feature \mathbf{Z}_c and the masked future frame visual feature \mathbf{Z}_f . We then concatenate \mathbf{Z}_f with the corresponding masking tokens that have the positional embedding added, resulting in \mathbf{Z}_f^d . Following this, \mathbf{Z}_f^d and \mathbf{Z}_c interact within the temporal decoder for decoding. The architecture of the temporal decoder block is in alignment with the standard transformer decoder block [89], consisting of a self-attention layer, a cross-attention layer, and a FFN layer. During decoding, the self-attention layer and FFN are solely used to process \mathbf{Z}_f^d . For the cross-attention layer, \mathbf{Z}_f^d is continuously updated as the query, while \mathbf{Z}_c , acting as the key and value, is kept constant. This asymmetric interact architecture is similar to the methods adopted in MultiMAE [3] and SiamMAE [33], and our experiment results show that it not only achieves more efficient training but also produces better results. Finally, with the decoded token sequence \mathbf{Z}_f^d , our temporal decoder predicts the invisible tokens of the future frame $\hat{\mathbf{I}}_f^d$, operating under the future frame masking map \mathbb{M}_f .

Multi-task Predictive Learning. As mentioned above, our STP jointly conducts spatiotemporal prediction by asymmetric masking ratio and dual decoders scheme, the whole decoding pipeline can be formally described as follows:

$$\begin{cases} \hat{\mathbf{I}}_c^d = \Phi_{dec_s}(\mathbf{Z}_c^d), \\ \hat{\mathbf{I}}_f^d = \Phi_{dec_t}(\mathbf{Z}_c, \mathbf{Z}_f^d). \end{cases} \quad (2)$$

Our loss function is the mean squared error (MSE) loss between the normalized masked pixels and the predicted pixels. So our loss function ℓ is as follows:

$$\ell = \text{MSE}(\hat{\mathbf{I}}_c, \mathbf{I}_c) + \text{MSE}(\hat{\mathbf{I}}_f, \mathbf{I}_f). \quad (3)$$

3.4 Downstream Policy Learning

To enable data and computation efficiency during the policy learning process, we adopt the paradigm of few-shot behavior cloning by learning from demonstrations (LfD), and we keep the image encoder frozen. Concretely, for each task, we are given offline expert demonstrations $\mathcal{S} = \{\tau_1, \dots, \tau_n\}$, where each τ_i is a trajectory of robot observations and actions, denoted as $\tau_i = [(o_0, a_0), \dots, (o_T, a_T)]$. Based on the \mathcal{S} , we train a policy model, $\pi_\theta(a|\mathcal{C}(\Phi_{enc}(o)))$, parameterized by θ , which maps from robot’s state representations to actions. Here, \mathcal{C} represents an optional concatenation operation that effectively fuses multi-view and multi-frame visual features, along with the robot’s proprioceptive state in the channel dimension. We optimize the π_θ through a standard behavior cloning MSE loss:

$$\min_{\theta} \sum_{(o,a) \sim \mathcal{S}} \text{MSE}(a, \pi_\theta(\mathcal{C}(\Phi_{enc}(o)))). \quad (4)$$

4 Experiments

4.1 Implementation on Pre-training

We execute pre-training with data from EgoVLP [55] for comprehensive ablation and fair comparison. It processes untrimmed videos of Ego4D and filters out that miss language narrations and belong to validation or test sets, resulting in a total of 3.8 million clips, called as Egoclip. We employ the vanilla vision transformers (ViT) [22] as our backbone. Additionally, we maintain consistency with prior works [73,59], directly using the [CLS] token as the global representation. The pre-training hyperparameters can be found in the supplementary materials.

4.2 Implementation on Downstream Policy

Evaluation Scheme. Following popular settings on PVRs for motor control [65,46,59], we adopt a computation and data-efficient few-shot behavior cloning paradigm by learning from demonstrations (LfD), and we freeze the visual representations when training the policy model. Specifically, for each task, we learn a policy π which is structured as a MLPs network. The policy models utilize both the history of visual observation embeddings and optional robot proprioceptive as inputs, subsequently generating executable actions as outputs. We optimize them through a standard behavior cloning MSE loss.

Simulation Tasks. We select the union of manipulation and locomotion tasks from prior works [65,59] for evaluation, encompassing 19 tasks across 5 simulated environments. These include Meta-World [104] (Assembly, Bin-Picking, Button-Press, Drawer-Open, and Hammer), Franka-Kitchen [31] (Sliding Door, Turning Light On, Opening Door, Turning Knob, and Opening Microwave), Adroit [74] (Relocate and Reorient-Pen), DMControl [83] (Finger-Spin, Reacher-Hard, Cheetah-Run, Walker-Stand, and Walker-Walk), and Trifinger [98] (Reach-Cube and Push-Cube). Similar to prior works [65,59], we establish all evaluation details such as the number of expert demonstrations and test trajectories, environmental viewpoints, optimization hyperparameters, seeds, history windows size, and the use of robot proprioceptive. These details can be found in the supplementary materials. For tasks in Meta-World, Franka-Kitchen, Adroit, and Trifinger, we report the maximum success rate, whereas for tasks in DMControl, we report the maximum reward score, rescaling to be in the range of [0, 100] by dividing by 10. Furthermore, we report the average metric across tasks for each environment, with specific task metric available in the supplementary materials, and the metric of each task is the average of all seeds and viewpoints.

Real-World Tasks. In our real-world experiments, we evaluate contact-rich picking and pouring tasks using a Franka Emika Research 3 robot arm in a table-top environment, ensuring no duplication with simulation Franka-Kitchen [31]. Specifically, we utilize four different camera views and resize their resolution uniformly to 224×224 . To effectively model the complex and multimodal action distribution in our real-world tasks, we select diffusion policy [16] as our policy model. In accordance with this approach, we concatenate the visual embeddings of all views from two sequential frames. For each task, we collect 100 noise demonstrations for training, and we conduct 20 trials per task during evaluation phase. The robotic arm and objects have different initial pose between training and testing. The evaluation demonstrations of our real-world tasks is shown in Figure 5. Please see supplementary materials for more setup details.

4.3 Performance on Downstream Simulation Tasks

In this section, we mainly analyze the performance of some pre-trained image representations on reproducible simulation tasks. Specifically, we first evaluate the following models: (1) public DINOv2 [67] that combines masked image modeling with self-distillation on large-scale image datasets; (2) public CLIP [71] that conducts contrastive learning on large-scale image-text pairs; (3) R3M-ViT trained based on Egoclip [55]; (4) public VC-1 [59]; (5) MAE trained based on Egoclip; (6) STP trained based on Egoclip. (7) STP that conducts hybrid pre-training with initialization using ImageNet-MAE [59]. Among them, (1) and (2) achieve excellent performance on core visual understanding tasks using zero-shot or linear probing evaluation settings. (3) and (4) utilize egocentric videos for robotic motor control. (5) and (7) are used for fair comparison and exploring the potential benefits of STP from more diverse image data, respectively.

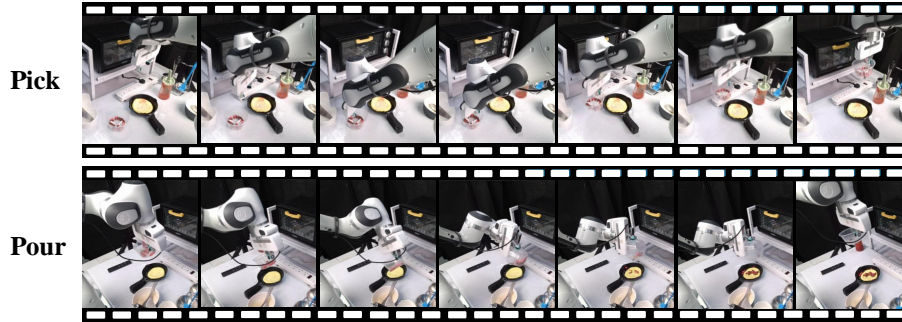


Fig. 2: **The evaluation demonstrations of our real-world tasks.** For picking, the robot arm needs to pick up the bowl on the desktop. For pouring, the robot arm needs to pour the ingredients from the bowl into the pot.

The experimental results are presented in Table 1. Consistent with prior findings [41, 59], there is no a universal foundation model that performs optimally across all benchmarks. However, on the whole, the MAE method is superior due to its effective modeling of low-level geometry and spatial structure, especially for the MetaWorld tasks that demand fine-grained control. Another intriguing observation is that MAE underperforms in the Franka-Kitchen and Adroit tasks. We believe that this could be due to its relatively weaker semantic representation. Under a fair comparison, our STP outperforms MAE by 4.1 (59.6 \rightarrow 63.7), and additionally benefits from a more diverse image data, improving by 0.5 (63.7 \rightarrow 64.2). This is attributed to that our STP not only captures static content features but also effectively models motion information by extracting temporal clues from videos of interactions and manipulations with the environment and objects. Additionally, we provide the visualization of the attention maps of several specific tasks in Figure 3. The results indicate that, on top of effectively capturing spatial information, our method further encourages the model to focus on motion areas or objects, thereby providing a more sparse and compact representation for downstream low-data imitation learning paradigm.

Finally, we also evaluate and compare the adaptation results of our representations to downstream motor control tasks. Specifically, we evaluate following settings: (a) The MAE pre-trained representation undergoes further MAE post-pre-training with task-specific data, and is frozen during policy training; (b) The STP pre-trained representation undergoes further STP post-pre-training with task-specific data, and is frozen during policy training; (c) The STP pre-trained representation undergoes end-to-end fine-tuning with task-specific data; (d) STP pre-training is performed directly using task-specific data and the resulting representation is frozen during policy training. The results show that end-to-end fine-tuning fails to yield the best results, suggesting that naively fine-tuning VIT-base could still lead to overfitting under few-shot behavior cloning scheme. Conversely, (a) and (b) achieve competitive results, with our STP achieving a 3.9

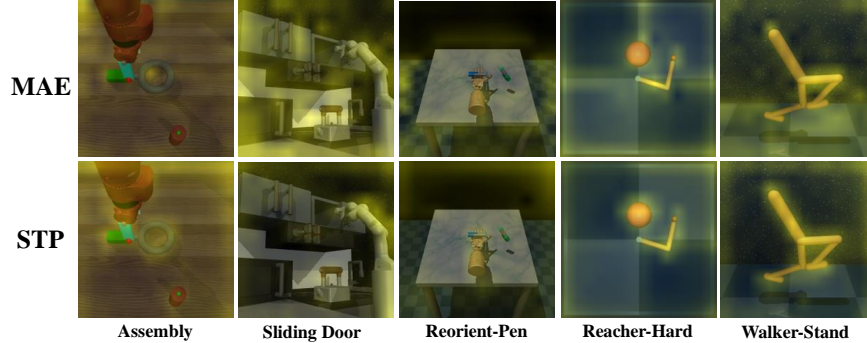


Fig. 3: **Attention Visualization.** We use the [CLS] token as query, average the attention of all heads at the last layer of the ViT encoder, and perform min-max normalization. We then upsample the attention map and overlay it on the original image, where the size of the attention value is directly proportional to the intensity of the yellow light. **Top:** MAE. **Bottom:** STP.

(72.5 \rightarrow 76.4) improvement on the weight average success rate than MAE, further demonstrating the effectiveness and data efficiency of our STP for in-domain data. Finally, the comparison between (a) and (d) also proves the effectiveness of pre-training with out-of-domain data.

4.4 Ablation on Downstream Simulation Tasks

In this section, we perform extensive ablation studies to further demonstrate the effectiveness of our joint spatial and temporal prediction, as well as temporal prediction condition design. In addition, we also study the influence of temporal decoder architecture design and future frame sampling strategy.

Current frame masking. The design of the current frame masking is crucial. On one hand, similar to MAE [38], masking some patches and predicting the missing parts can effectively promote the learning of image content features. On the other hand, the visible patches of the current frame need to interact with the condition to predict the future frame. Specifically, we mask the current frame at masking rates of 75%, 50%, and 0%, respectively, and optionally predict the missing parts through the spatial decoder. The results are shown in Table 2. From results, we see that the masking ratio of 75% and performing spatial prediction still lead to the best performance. This demonstrates the importance of retaining MAE [38] for content features learning, especially for low-level manipulation in Meta-World, while a current frame with a high masking ratio (75%) is sufficient to interact with other conditions to predict the future frame.

Temporal prediction condition design. Subsequently, we discuss the influence of temporal prediction condition design. We implicitly model motion in actionless video data by predicting the pixels of the future frame. A direct and simple idea is to use language narration as a condition. The text tokens can

Table 1: Performance comparisons of visual representations on simulation benchmarks. We report the average score across all tasks for each simulation environment. DINOv2 uses **ViT-B/14**, CLIP uses **ViT-B/32**, and others use **ViT-B/16**. Mt-Wd, Fr-Ki, DMC, Adro, Tr-fi, and WA respectively represent MetaWorld, Franka-Kitchen, DMControl, Adroit, Trifinger, and weight average. * denotes that public VC-1 samples image frames from full Ego4D dataset.

	Pre-training Data	Mt-Wd	Fr-Ki	DMC	Adro	Tr-fi	WA
DINOv2 [67]	LVD-142M	77.9	41.2	59.4	50.7	69.0	59.6
CLIP [71]	Image-text pairs	75.5	39.8	52.2	51.3	57.7	55.6
R3M [65]	Ego	81.3	30.6	52.2	46.7	64.7	54.9
VC-1 [59]	Ego*+MNI	88.8	38.4	60.9	46.0	70.5	61.8
MAE [38]	Ego	85.1	36.7	59.2	43.4	70.6	59.6
STP	Ego	92.0	40.9	62.1	48.0	69.3	63.7
STP	Ego+I	94.1	42.5	61.6	47.3	66.7	64.2
MAE (Post PT)	Ego+Demo	93.6	46.9	81.1	58.0	76.8	72.5
STP (Post PT)	Ego+Demo	97.3	53.6	82.8	63.3	78.0	76.4
STP (E2E FT)	Ego	87.2	52.4	55.2	40.0	70.4	62.9
STP	Demo	70.3	30.4	52.5	38.0	70.8	51.8

be flexibly utilized as inputs to ViT [22], forming a multimodal encoder. Language narration provides a high-level behavior description, but lacks low-level visual dynamic priors for pixel-level prediction. However, leaking part of the future frame can effectively provide these priors. In order to explore how to construct a more meaningful temporal prediction proxy task, we compare the following schemes: (1) only language narration, (2) masking 95% of the future frame, (3) masking 90% of the future frame, (4) masking 95% of the future frame and language narration, and (5) masking 95% of the future frame and language narration, but the language is added in the temporal decoder, instead of being fused with the visible image patches in the multimodal encoder. We tokenize all language narration by pre-trained DistilBERT [75]. The results are shown in Table 3. From results, we see that using only language as a prediction condition leads to a significant decline in performance, while leaking a small amount of future frame (masking 95%) in the temporal decoder can achieve competitive results. As for joint conditions of language and future frame with 95% masking ratio, adding language in the encoder is better than in the decoder. Additionally, adding language performs better on DMControl (64.1 vs. 62.1) and Trifinger (70.8 vs. 69.3), while not adding language performs better on Meta-World (92.0

Table 2: The ablation of the current frame masking and spatial prediction.

ρ^c	Predict	MetaWorld	Frank-Kitchen	DMControl	Adroit	Trifinger	Weight Average
75%	✓	92.0	40.9	62.1	48.0	69.3	63.7
75%		84.5	34.7	55.4	43.3	65.3	57.4
50%	✓	82.1	36.0	60.3	48.0	66.8	59.0
0%		79.2	39.7	54.8	44.0	63.1	57.0

Table 3: The ablation of temporal prediction condition design.

Condition	MetaWorld	Frank-Kitchen	DMControl	Adroit	Trifinger	Weight Average
L-E	82.1	30.7	55.5	42.0	63.8	55.4
95%	92.0	40.9	62.1	48.0	69.3	63.7
90%	91.2	42.5	62.8	44.7	65.9	63.4
L-E + 95%	91.0	37.7	64.1	46.7	70.8	63.1
L-D + 95%	88.0	34.3	62.6	46.7	69.3	60.9

vs. 91.0), Franka-Kitchen (40.9 vs. 37.7) and Adroit (48.0 vs. 46.7). We speculate the reasons for language hurts performance are as follows: (i) The input gap (multi-modal and single-modal) between upstream and downstream; (ii) Extra language in ViT may result in the loss of some fine-grained information capture. Furthermore, the latter does not require language supervision, and can provide a more scalable self-supervised solution.

Temporal decoder architecture design. We also investigate the impact of the temporal decoder architecture design. Specifically, we consider two types of decoder blocks. One is the joint-self architecture, where each block includes a self-attention layer and FFN layer. Similar joint architecture has been adopted in [26,102], where the visible tokens of the current frame, the visible tokens of the future frame, and learnable masking tokens perform global self-attention. The other is the self-cross architecture, each block includes a self-attention layer, a cross-attention layer, and FFN layer, similar architecture has been adopted in [3,33]. In cross-attention layer, the visible tokens of the current frame act as key and value, while the visible tokens and masking tokens of the future frame act as query. We consider the following settings: (1) 8 joint-self decoder blocks, (2) 12 joint-self decoder blocks, (3) 8 self-cross decoder blocks. Among them, setting (2) and (3) have similar amounts of parameters for a fairer comparison. The results are shown in Table 4. The results show that the self-cross decoder block obtains the best performance. We speculate that this is because it ensures that the past frame tokens will not be updated in the temporal decoder and are specifically used for temporal correlation.

Table 4: The ablation of temporal decoder architecture design.

Decoder	MetaWorld	Frank-Kitchen	DMControl	Adroit	Trifinger	Weight Average
8 joint-self	87.7	36.9	55.7	46.0	71.3	59.8
12 joint-self	88.5	35.0	55.7	46.0	67.0	59.1
8 self-cross	92.0	40.9	62.1	48.0	69.3	63.7

Frame sampling strategy. Finally, we investigate the impact of the sampling strategy between the current frame and future frame. The difficulty of temporal prediction is directly proportional to the frame interval values. We establish four settings where we fix the sampling intervals at 8, 16, and 24 respectively, and for the fourth setting, we randomly select an interval within the range of [8, 24]. The

Table 5: The ablation of frame sampling strategy.

Frame interval	MetaWorld	Frank-Kitchen	DMControl	Adroit	Trifinger	Weight Average
8	89.6	39.9	58.4	46.0	67.0	61.3
16	92.0	40.9	62.1	48.0	69.3	63.7
24	89.1	41.1	61.5	46.0	68.1	62.5
8, 24	92.3	37.1	57.3	42.0	68.4	60.8

Table 6: Performance comparisons on real-world tasks.

Method	Picking	Pouring	Average
MAE	65.0	45.0	55.0
STP	65.0	65.0	65.0

results are shown in Table 5. The results show that an interval of 16 achieves the best balance for building temporal prediction proxy task.

4.5 Performance on Downstream Real-world Tasks

In this section, we report our experiment results on real-world picking and pouring tasks. We report the average success rate for each task. Specifically, we compare STP with the baseline MAE, both of which are trained on out-of-domain videos and kept frozen during policy training. The results are shown in Table 6. From the results, it can be seen that STP has achieved significant advantages in the pouring task. It can more accurately align with the moving bowl and the pot. In addition, although MAE and STP have a same success rate in picking tasks, STP tends to execute grasping in a better position. This indicates that the trend and conclusion of our STP are consistent in both simulation and the real-world, which also aligns with the findings of [79].

5 Conclusion

In this work, we propose STP, a simple, efficient and effective self-supervised visual representation pre-training framework for robotic motor control. Our STP jointly performs spatiotemporal predictive learning on large-scale videos within a multi-task learning manner. Our STP captures content features by predicting the invisible areas within the masked current frame, and simultaneously captures motion features by using a future frame with an extremely high masking ratio as a condition to predict the invisible areas within that future frame. We carry out the largest-scale evaluation of PVRs for robotic motor control to date to demonstrate the effectiveness of STP. Furthermore, as for pre-training data, we also prove that extending STP to hybrid pre-training and post-pre-training could further unleash its generality and data efficiency.

6 Limitations and Discussion

Although STP has demonstrated superior performance in extensive experiments, there remain some challenges and future works. From the perspective of pre-training data, Ego4D provides numerous human-object interaction scenes and good motion clues. Building larger-scale and more diverse potential datasets such as [63,30] to scale up STP is worth exploring. Regarding pre-training methods, exploring predictive targets outside of pixel space and more effective sampling and masking strategies present intriguing research directions. From an evaluation standpoint, we utilize a frozen ViT to extract agent state representations and adopt the paradigm of few-shot behavior cloning, other policy learning methods (reinforcement learning, visual reward function, visual task specification), have not been explored. In conclusion, as the first method of performing temporal prediction on large-scale videos for self-supervised visual representation learning intended for robotic motor control tasks, we hope STP can be taken as a strong baseline and facilitate further research along this direction.

7 Appendix

7.1 Pre-training Details

In this section, we describe the details of our STP pre-training. Specifically, we list some key training and architectural hyperparameters of STP in Table 7. In addition, as for our MAE [38] baseline, we mainly follow the publicly available code of MAE⁴ and train the same number of epochs for fair comparison. Finally, we also provide some prediction results in Figure 4.

7.2 Simulation Environments Details

In this section, we first present further details of the STP post-pre-training on downstream simulation environments. Subsequently, we delineate the specific hyperparameters used in the behavior cloning policy training within these simulation environments. Finally, we provide the comprehensive evaluation scheme for each simulation environment.

In regards to the STP post-pre-training, we utilize data that aligns with the policy training, and the specific architecture hyperparameters correspond to those listed in Table 7. Depending on the specific demonstration data, we adjust the values of total epochs, warmup epochs, effective batch size, and the frame interval, as shown in Table 8. As for policy training and evaluation schemes, we primarily refer to the publicly available code⁵ and training data of VC-1 [59] for Metaworld [104], DMControl [83], Adroit [74] and Trifinger [98]. Similarly, for Franka-Kitchen [31], we follow the public code⁶ and training data of R3M [65].

⁴ <https://github.com/facebookresearch/mae>

⁵ <https://github.com/facebookresearch/eai-vc/tree/main/cortexbench>

⁶ <https://github.com/facebookresearch/r3m/tree/eval/evaluation>

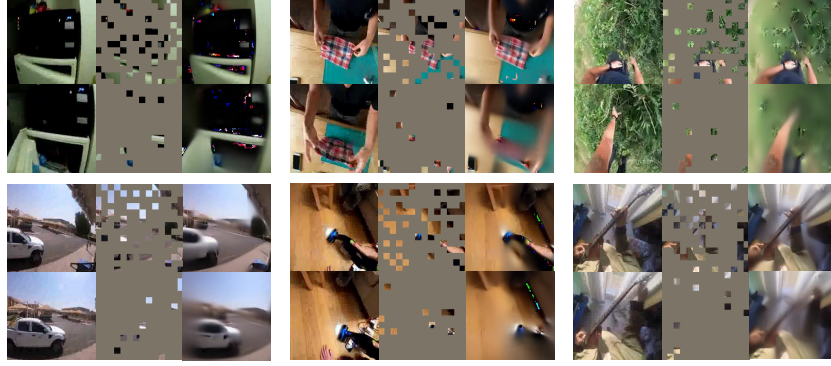


Fig. 4: Some examples of our STP prediction result on Ego4D videos. For each six tuple, we show the ground-truth (left), masked frames (middle), STP prediction results (right), current frames (top), and future frames (bottom). We simply overlay the output with the visible patches to improve visual quality.

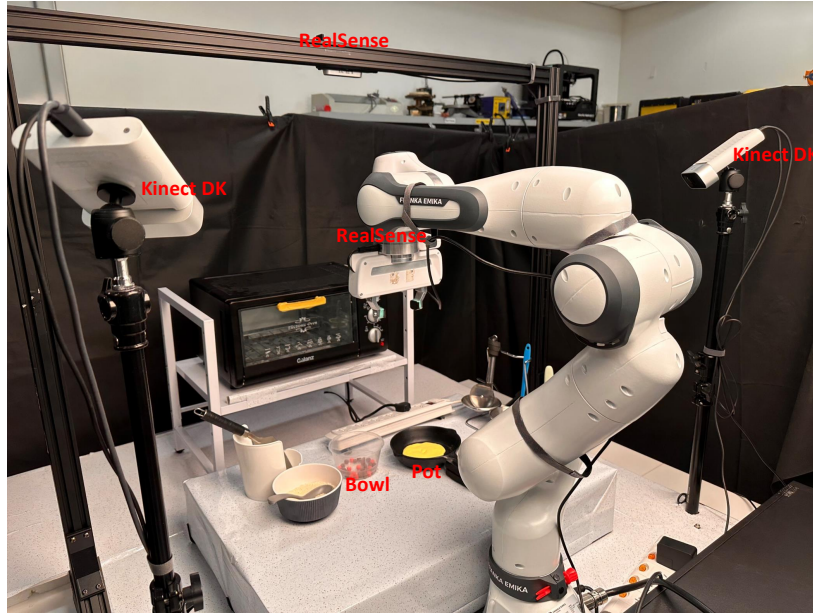


Fig. 5: Our real-world scene with four cameras and a Franka Emika robot arm.

Table 7: Training and architectural hyperparameters for STP pre-training.

Hyperparameter	Value
<i>STP Pre-training</i>	
optimizer	AdamW [49]
base learning rate	0.00015
weight decay	0.05
optimizer momentum	$\beta_1, \beta_2 = 0.9, 0.95$
effective batch size	4096
learning rate schedule	cosine decay
total epochs	50
warmup epochs	5
augmentation	RandomResizedCrop (0.8, 1)
<i>Encoder ViT-base Architecture</i>	
patch size	16
#layers	12
#MHSA heads	12
hidden dim	768
positional embedding	sin-cos initialization and fix
<i>Dual Decoder ViT-base Architecture</i>	
#layers	8
#MHSA heads	16
hidden dim	512
positional embedding	sin-cos initialization and fix

Specifically, the policy training hyperparameters and evaluation schemes are shown in Table 9 and Table 10, respectively. About policy training, we completely follow the setting of prior works [65, 59] when freezing the encoder; when performing end-to-end fine-tuning, we make appropriate adjustments to the batch size and learning rate. As to evaluation details, the term ‘prop.’ stands for whether proprioceptive information is used or not, and ‘history window size’ signifies the number of frames received by the policy model at each step, with features between frames being fused through concatenation. ‘Number of trajectories’ represents the quantity of trajectories evaluated. In addition, it is worth noting that the metrics we report are the average value across all seeds and camera view-

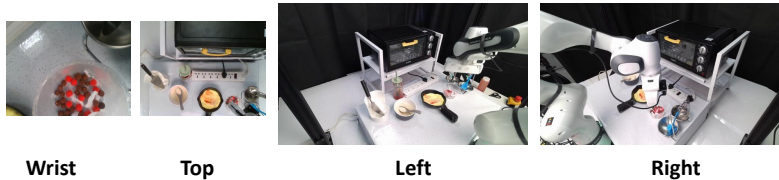


Fig. 6: An example of four views.

points. Finally, we also report the results of our post-pre-training STP on each task in Table 11.

7.3 Real-World Environments Details

In this section, we outline the details of our real-world setup and evaluation scheme. As depicted in Figure 5, our real-world scenario includes four camera viewpoints: top, left, right, and wrist. It includes two Kinect DK and two RealSense cameras. An example of four views is shown in Figure 6. Following the approach in [27], we collect robot data using a VR tele-operation setup. In this way, we collect 100 continuous trajectories for each task. It is worth noting that the quality of these demonstrations leaves room for improvement and contains a lot of noise. During the evaluation phase, we primarily evaluate two contact-rich tasks that have not appeared in Franka-Kitchen [31] benchmark: (1) Picking. It requires the robot arm to pick up the transparent bowl off the table; (2) Pouring. It requires the robot arm to pour at least three-quarter of the ingredients from the transparent bowl into the black pot. For each task, we change the initial pose of the robot arm and objects within a certain range as well as conduct 20 trials. In addition, there are different distractors on the desktop during training and testing, which also evaluates the robustness of the model to distractors. Throughout the process, we use ROS and MoveIt for hardware communication and motion planning.

Table 8: STP post-pre-training hyperparameters on simulation environments.

	MetaWorld	Franka-Kitchen	DMControl	Adroit	Trifinger
total epochs	50	100	50	50	50
warmup epochs	5	5	5	5	5
effective batch size	1024	128	2048	1024	1024
number of demonstrations	25	25	100	100	100
frame interval	4	4	4	4	16

Table 9: Policy training hyperparameters on simulation environments.

		MetaWorld	Franka-Kitchen	DMControl	Adroit	Trifinger
epochs		100	480	100	100	100 / 1000
batch size	frozen	256	32	256	256	32
	fine-tuning	64	32	64	64	16
learning rate	frozen	0.001	0.001	0.001	0.001	0.0001
	fine-tuning	0.00005	0.0001	0.00005	0.00005	0.0001

Table 10: Evaluation schemes on simulation environments.

Benchmark	Observation Space	History Window Size	Camera ViewPoints	Seeds	Number of Trajectories
Metaworld	RGB + prop.	3	top_cap2	100, 200, 300	25
Franka-Kitchen	RGB + prop.	1	left, right	123, 124, 125	50
DMControl	RGB	3	0	100, 200, 300	25
Adroit	RGB + prop.	1	vil_camera	100, 200, 300	25
Trifinger	RGB + prop.	1	default	10	25

Table 11: The success rate for each task on simulation bechmarks.

Assembly	Bin-Picking	Button-Press	Drawer-Open	Hammer
94.7	97.3	94.7	100.0	100.0
Sliding Door	Turning Light on	Opening Door	Turning Knob	Opening Microwave
96.0	72.7	39.0	31.3	29.0
Relocate	Reorient-Pen	Finger-Spin	Cheetah-Run	Reacher-Hard
49.3	77.3	69.6	71.9	87.7
Walker-Stand	Walker-Walk	Reach-Cube	Push-Cube	
95.9	89.0	85.3	70.6	

References

- Andrychowicz, O.M., Baker, B., Chociej, M., Jozefowicz, R., McGrew, B., Pachocki, J., Petron, A., Plappert, M., Powell, G., Ray, A., et al.: Learning dexterous in-hand manipulation. *IJRR* **39**(1), 3–20 (2020) [2](#)
- Assran, M., Duval, Q., Misra, I., Bojanowski, P., Vincent, P., Rabbat, M., LeCun, Y., Ballas, N.: Self-supervised learning from images with a joint-embedding predictive architecture. In: *CVPR*. pp. 15619–15629 (2023) [2](#), [4](#)
- Bachmann, R., Mizrahi, D., Atanov, A., Zamir, A.: Multimaes: Multi-modal multi-task masked autoencoders. In: *ECCV*. pp. 348–367. Springer (2022) [7](#), [13](#)
- Baevski, A., Hsu, W.N., Xu, Q., Babu, A., Gu, J., Auli, M.: Data2vec: A general framework for self-supervised learning in speech, vision and language. In: *ICML*. pp. 1298–1312. PMLR (2022) [4](#)
- Bahl, S., Gupta, A., Pathak, D.: Human-to-robot imitation in the wild. In: Hauser, K., Shell, D.A., Huang, S. (eds.) *RSS* (2022). <https://doi.org/10.15607/RSS.2022.XVIII.026>, <https://doi.org/10.15607/RSS.2022.XVIII.026> [4](#)
- Bahl, S., Mendonca, R., Chen, L., Jain, U., Pathak, D.: Affordances from human videos as a versatile representation for robotics. In: *CVPR*. pp. 13778–13790 (2023) [4](#)
- Bao, H., Dong, L., Piao, S., Wei, F.: Beit: Bert pre-training of image transformers. In: *ICLR* (2021) [3](#), [4](#)
- Bardes, A., Ponce, J., LeCun, Y.: Mc-jepa: A joint-embedding predictive architecture for self-supervised learning of motion and content features. *arXiv preprint arXiv:2307.12698* (2023) [4](#)
- Bousmalis, K., Vezzani, G., Rao, D., Devin, C., Lee, A.X., Bauza, M., Davchev, T., Zhou, Y., Gupta, A., Raju, A., et al.: Robocat: A self-improving foundation agent for robotic manipulation. *arXiv preprint arXiv:2306.11706* (2023) [4](#)

10. Brohan, A., Brown, N., Carbajal, J., Chebotar, Y., Chen, X., Choromanski, K., Ding, T., Driess, D., Dubey, A., Finn, C., et al.: Rt-2: Vision-language-action models transfer web knowledge to robotic control. In: CoRL (2023) [5](#)
11. Brohan, A., Brown, N., Carbajal, J., Chebotar, Y., Dabis, J., Finn, C., Gopalakrishnan, K., Hausman, K., Herzog, A., Hsu, J., Ibarz, J., Ichter, B., Irpan, A., Jackson, T., Jesmonth, S., Joshi, N.J., Julian, R., Kalashnikov, D., Kuang, Y., Leal, I., Lee, K., Levine, S., Lu, Y., Malla, U., Manjunath, D., Mordatch, I., Nachum, O., Parada, C., Peralta, J., Perez, E., Pertsch, K., Quiambao, J., Rao, K., Ryoo, M.S., Salazar, G., Sanketi, P.R., Sayed, K., Singh, J., Son-takke, S., Stone, A., Tan, C., Tran, H.T., Vanhoucke, V., Vega, S., Vuong, Q., Xia, F., Xiao, T., Xu, P., Xu, S., Yu, T., Zitkovich, B.: RT-1: robotics transformer for real-world control at scale. In: Bekris, K.E., Hauser, K., Herbert, S.L., Yu, J. (eds.) RSS (2023). <https://doi.org/10.15607/RSS.2023.XIX.025>, <https://doi.org/10.15607/RSS.2023.XIX.025> [5](#)
12. Cai, S., Wang, Z., Ma, X., Liu, A., Liang, Y.: Open-world multi-task control through goal-aware representation learning and adaptive horizon prediction. In: CVPR. pp. 13734–13744 (2023) [4](#)
13. Caron, M., Touvron, H., Misra, I., Jégou, H., Mairal, J., Bojanowski, P., Joulin, A.: Emerging properties in self-supervised vision transformers. In: ICCV. pp. 9650–9660 (2021) [4](#)
14. Chen, T., Kornblith, S., Norouzi, M., Hinton, G.: A simple framework for contrastive learning of visual representations. In: ICML. pp. 1597–1607. PMLR (2020) [4](#)
15. Chen, X., Xie, S., He, K.: An empirical study of training self-supervised vision transformers. in 2021 ieee. In: ICCV. pp. 9620–9629 [2](#), [4](#)
16. Chi, C., Feng, S., Du, Y., Xu, Z., Cousineau, E., Burchfiel, B., Song, S.: Diffusion policy: Visuomotor policy learning via action diffusion. In: Bekris, K.E., Hauser, K., Herbert, S.L., Yu, J. (eds.) RSS (2023). <https://doi.org/10.15607/RSS.2023.XIX.026>, <https://doi.org/10.15607/RSS.2023.XIX.026> [9](#)
17. Cui, Y., Jiang, C., Wu, G., Wang, L.: Mixformer: End-to-end tracking with iterative mixed attention. arXiv preprint arXiv:2302.02814 (2023) [4](#)
18. Dai, Y., Yang, M., Dai, B., Dai, H., Nachum, O., Tenenbaum, J., Schuurmans, D., Abbeel, P.: Learning universal policies via text-guided video generation. arXiv preprint arXiv:2302.00111 (2023) [4](#)
19. Dasari, S., Srirama, M.K., Jain, U., Gupta, A.: An unbiased look at datasets for visuo-motor pre-training. In: CoRL (2023) [2](#), [3](#), [4](#)
20. Deng, J., Dong, W., Socher, R., Li, L.J., Li, K., Fei-Fei, L.: Imagenet: A large-scale hierarchical image database. In: CVPR. pp. 248–255. Ieee (2009) [3](#)
21. Derrington, A., Lennie, P.: Spatial and temporal contrast sensitivities of neurones in lateral geniculate nucleus of macaque. *The Journal of physiology* **357**(1), 219–240 (1984) [2](#)
22. Dosovitskiy, A., Beyer, L., Kolesnikov, A., Weissenborn, D., Zhai, X., Unterthiner, T., Dehghani, M., Minderer, M., Heigold, G., Gelly, S., Uszkoreit, J., Houlsby, N.: An image is worth 16x16 words: Transformers for image recognition at scale. In: ICLR [2](#), [4](#), [6](#), [8](#), [12](#)
23. Du, Y., Yang, M., Florence, P., Xia, F., Wahid, A., Ichter, B., Sermanet, P., Yu, T., Abbeel, P., Tenenbaum, J.B., et al.: Video language planning. arXiv preprint arXiv:2310.10625 (2023) [4](#)
24. Fang, H.S., Fang, H., Tang, Z., Liu, J., Wang, C., Wang, J., Zhu, H., Lu, C.: Rh20t: A comprehensive robotic dataset for learning diverse skills in one-shot. In:

- Towards Generalist Robots: Learning Paradigms for Scalable Skill Acquisition@ CoRL2023 (2023) 5
25. Fang, Y., Wang, W., Xie, B., Sun, Q., Wu, L., Wang, X., Huang, T., Wang, X., Cao, Y.: Eva: Exploring the limits of masked visual representation learning at scale. In: CVPR. pp. 19358–19369 (2023) 2
 26. Geng, X., Liu, H., Lee, L., Schuurams, D., Levine, S., Abbeel, P.: Multi-modal masked autoencoders learn transferable representations. arXiv preprint arXiv:2205.14204 (2022) 13
 27. George, A., Bartsch, A., Farimani, A.B.: Openvr: Teleoperation for manipulation. arXiv preprint arXiv:2305.09765 (2023) 18
 28. Girdhar, R., Grauman, K.: Anticipative video transformer. In: ICCV. pp. 13505–13515 (2021) 4
 29. Grauman, K., Westbury, A., Byrne, E., Chavis, Z., Furnari, A., Girdhar, R., Hamburger, J., Jiang, H., Liu, M., Liu, X., et al.: Ego4d: Around the world in 3,000 hours of egocentric video. In: CVPR. pp. 18995–19012 (2022) 2
 30. Grauman, K., Westbury, A., Torresani, L., Kitani, K., Malik, J., Afouras, T., Ashutosh, K., Baiyya, V., Bansal, S., Boote, B., et al.: Ego-exo4d: Understanding skilled human activity from first-and third-person perspectives. arXiv preprint arXiv:2311.18259 (2023) 15
 31. Gupta, A., Kumar, V., Lynch, C., Levine, S., Hausman, K.: Relay policy learning: Solving long-horizon tasks via imitation and reinforcement learning. In: CoRL. pp. 1025–1037. PMLR (2020) 9, 15, 18
 32. Gupta, A., Tian, S., Zhang, Y., Wu, J., Martín-Martín, R., Fei-Fei, L.: Maskvit: Masked visual pre-training for video prediction. In: ICLR (2022) 4
 33. Gupta, A., Wu, J., Deng, J., Fei-Fei, L.: Siamese masked autoencoders (2023) 4, 7, 13
 34. Ha, H., Florence, P., Song, S.: Scaling up and distilling down: Language-guided robot skill acquisition. In: Conference on Robot Learning. pp. 3766–3777. PMLR (2023) 5
 35. Han, T., Xie, W., Zisserman, A.: Video representation learning by dense predictive coding. In: ICCV Workshops. pp. 0–0 (2019) 4
 36. Hansen, N., Yuan, Z., Ze, Y., Mu, T., Rajeswaran, A., Su, H., Xu, H., Wang, X.: On pre-training for visuo-motor control: Revisiting a learning-from-scratch baseline. arXiv preprint arXiv:2212.05749 (2022) 4
 37. Harvey, W., Naderiparizi, S., Masrani, V., Weillbach, C., Wood, F.: Flexible diffusion modeling of long videos. NeurIPS 35, 27953–27965 (2022) 4
 38. He, K., Chen, X., Xie, S., Li, Y., Dollár, P., Girshick, R.: Masked autoencoders are scalable vision learners. In: CVPR. pp. 16000–16009 (2022) 2, 4, 6, 11, 12, 15
 39. He, K., Fan, H., Wu, Y., Xie, S., Girshick, R.: Momentum contrast for unsupervised visual representation learning. In: CVPR. pp. 9729–9738 (2020) 4
 40. He, K., Zhang, X., Ren, S., Sun, J.: Deep residual learning for image recognition. In: CVPR. pp. 770–778 (2016) 3, 4
 41. Hu, Y., Wang, R., Li, L.E., Gao, Y.: For pre-trained vision models in motor control, not all policy learning methods are created equal. arXiv preprint arXiv:2304.04591 (2023) 4, 10
 42. Jang, E., Irpan, A., Khansari, M., Kappler, D., Ebert, F., Lynch, C., Levine, S., Finn, C.: BC-Z: zero-shot task generalization with robotic imitation learning. In: Faust, A., Hsu, D., Neumann, G. (eds.) CoRL. Proceedings of Machine Learning Research, vol. 164, pp. 991–1002. PMLR (2021) 4, 5

43. Jin, C., Tan, W., Yang, J., Liu, B., Song, R., Wang, L., Fu, J.: Alphablock: Embodied finetuning for vision-language reasoning in robot manipulation. arXiv preprint arXiv:2305.18898 (2023) [5](#)
44. Jing, Y., Zhu, X., Liu, X., Sima, Q., Yang, T., Feng, Y., Kong, T.: Exploring visual pre-training for robot manipulation: Datasets, models and methods. arXiv preprint arXiv:2308.03620 (2023) [4](#)
45. Ju, Y., Hu, K., Zhang, G., Zhang, G., Jiang, M., Xu, H.: Robo-abc: Affordance generalization beyond categories via semantic correspondence for robot manipulation. arXiv preprint arXiv:2401.07487 (2024) [4](#)
46. Karamcheti, S., Nair, S., Chen, A.S., Kollar, T., Finn, C., Sadigh, D., Liang, P.: Language-driven representation learning for robotics. In: Bekris, K.E., Hauser, K., Herbert, S.L., Yu, J. (eds.) RSS (2023). <https://doi.org/10.15607/RSS.2023.XIX.032>, <https://doi.org/10.15607/RSS.2023.XIX.032> [3](#), [4](#), [8](#)
47. Kim, H., Ohmura, Y., Kuniyoshi, Y.: Multi-task robot data for dual-arm fine manipulation. arXiv preprint arXiv:2401.07603 (2024) [4](#)
48. Kim, M.J., Wu, J., Finn, C.: Giving robots a hand: Learning generalizable manipulation with eye-in-hand human video demonstrations. arXiv preprint arXiv:2307.05959 (2023) [4](#)
49. Kingma, D.P., Ba, J.: Adam: A method for stochastic optimization. arXiv preprint arXiv:1412.6980 (2014) [17](#)
50. Kleinschmidt, A., Thilo, K.V., Büchel, C., Gresty, M.A., Bronstein, A.M., Frackowiak, R.S.: Neural correlates of visual-motion perception as object-or self-motion. *Neuroimage* **16**(4), 873–882 (2002) [2](#)
51. Ko, P.C., Mao, J., Du, Y., Sun, S.H., Tenenbaum, J.B.: Learning to act from actionless videos through dense correspondences. arXiv preprint arXiv:2310.08576 (2023) [4](#)
52. Kong, X., Zhang, X.: Understanding masked image modeling via learning occlusion invariant feature. In: CVPR. pp. 6241–6251 (2023) [3](#)
53. Levine, S., Finn, C., Darrell, T., Abbeel, P.: End-to-end training of deep visuomotor policies. *JMLR* **17**(1), 1334–1373 (2016) [2](#)
54. Li, X., Liu, M., Zhang, H., Yu, C., Xu, J., Wu, H., Cheang, C., Jing, Y., Zhang, W., Liu, H., et al.: Vision-language foundation models as effective robot imitators. arXiv preprint arXiv:2311.01378 (2023) [5](#)
55. Lin, K.Q., Wang, J., Soldan, M., Wray, M., Yan, R., XU, E.Z., Gao, D., Tu, R.C., Zhao, W., Kong, W., et al.: Egocentric video-language pretraining. *NeurIPS* **35**, 7575–7586 (2022) [2](#), [8](#), [9](#)
56. Lin, X., So, J., Mahalingam, S., Liu, F., Abbeel, P.: Spawnnet: Learning generalizable visuomotor skills from pre-trained networks. arXiv preprint arXiv:2307.03567 (2023) [4](#)
57. Ma, Y.J., Liang, W., Som, V., Kumar, V., Zhang, A., Bastani, O., Jayaraman, D.: Liv: Language-image representations and rewards for robotic control. arXiv preprint arXiv:2306.00958 (2023) [4](#)
58. Ma, Y.J., Sodhani, S., Jayaraman, D., Bastani, O., Kumar, V., Zhang, A.: Vip: Towards universal visual reward and representation via value-implicit pre-training. In: ICLR (2023) [2](#), [4](#)
59. Majumdar, A., Yadav, K., Arnaud, S., Ma, Y.J., Chen, C., Silwal, S., Jain, A., Berges, V.P., Abbeel, P., Malik, J., et al.: Where are we in the search for an artificial visual cortex for embodied intelligence? (2023) [2](#), [3](#), [4](#), [8](#), [9](#), [10](#), [12](#), [15](#), [17](#)

60. Marza, P., Matignon, L., Simonin, O., Wolf, C.: Task-conditioned adaptation of visual features in multi-task policy learning. arXiv preprint arXiv:2402.07739 (2024) 4
61. Mathieu, M., Couprie, C., LeCun, Y.: Deep multi-scale video prediction beyond mean square error. arXiv preprint arXiv:1511.05440 (2015) 4
62. Mendonca, R., Bahl, S., Pathak, D.: Structured world models from human videos. In: Bekris, K.E., Hauser, K., Herbert, S.L., Yu, J. (eds.) RSS (2023). <https://doi.org/10.15607/RSS.2023.XIX.012>, <https://doi.org/10.15607/RSS.2023.XIX.012> 4
63. Miech, A., Zhukov, D., Alayrac, J.B., Tapaswi, M., Laptev, I., Sivic, J.: Howto100m: Learning a text-video embedding by watching hundred million narrated video clips. In: CVPR. pp. 2630–2640 (2019) 15
64. Mu, Y., Zhang, Q., Hu, M., Wang, W., Ding, M., Jin, J., Wang, B., Dai, J., Qiao, Y., Luo, P.: EmbodiedGPT: Vision-language pre-training via embodied chain of thought. In: NeurIPS (2023) 5
65. Nair, S., Rajeswaran, A., Kumar, V., Finn, C., Gupta, A.: R3m: A universal visual representation for robot manipulation. In: CoRL (2022) 2, 3, 4, 8, 9, 12, 15, 17
66. Oord, A.v.d., Li, Y., Vinyals, O.: Representation learning with contrastive predictive coding. arXiv preprint arXiv:1807.03748 (2018) 4
67. Oquab, M., Darcet, T., Moutakanni, T., Vo, H., Szafraniec, M., Khalidov, V., Fernandez, P., Haziza, D., Massa, F., El-Nouby, A., et al.: Dinov2: Learning robust visual features without supervision. arXiv preprint arXiv:2304.07193 (2023) 2, 4, 9, 12
68. Padalkar, A., Pooley, A., Jain, A., Bewley, A., Herzog, A., Irpan, A., Khazatsky, A., Rai, A., Singh, A., Brohan, A., et al.: Open x-embodiment: Robotic learning datasets and rt-x models. arXiv preprint arXiv:2310.08864 (2023) 5
69. Parisi, S., Rajeswaran, A., Purushwalkam, S., Gupta, A.: The unsurprising effectiveness of pre-trained vision models for control. In: ICML. pp. 17359–17371. PMLR (2022) 2, 3, 4
70. Qin, Y., Wu, Y.H., Liu, S., Jiang, H., Yang, R., Fu, Y., Wang, X.: Dexmv: Imitation learning for dexterous manipulation from human videos. In: ECCV. pp. 570–587. Springer (2022) 4
71. Radford, A., Kim, J.W., Hallacy, C., Ramesh, A., Goh, G., Agarwal, S., Sastry, G., Askell, A., Mishkin, P., Clark, J., et al.: Learning transferable visual models from natural language supervision. In: ICLR. pp. 8748–8763. PMLR (2021) 2, 3, 9, 12
72. Radosavovic, I., Shi, B., Fu, L., Goldberg, K., Darrell, T., Malik, J.: Robot learning with sensorimotor pre-training (2023) 4
73. Radosavovic, I., Xiao, T., James, S., Abbeel, P., Malik, J., Darrell, T.: Real-world robot learning with masked visual pre-training. In: CoRL. pp. 416–426. PMLR (2023) 2, 4, 8
74. Rajeswaran, A., Kumar, V., Gupta, A., Vezzani, G., Schulman, J., Todorov, E., Levine, S.: Learning complex dexterous manipulation with deep reinforcement learning and demonstrations. RSS (2018) 9, 15
75. Sanh, V., Debut, L., Chaumond, J., Wolf, T.: Distilbert, a distilled version of bert: smaller, faster, cheaper and lighter. arXiv preprint arXiv:1910.01108 (2019) 12
76. Seo, Y., Hafner, D., Liu, H., Liu, F., James, S., Lee, K., Abbeel, P.: Masked world models for visual control. In: CoRL. pp. 1332–1344. PMLR (2023) 4

77. Seo, Y., Lee, K., James, S.L., Abbeel, P.: Reinforcement learning with action-free pre-training from videos. In: ICML. pp. 19561–19579. PMLR (2022) [4](#)
78. Sharma, M., Fantacci, C., Zhou, Y., Koppula, S., Heess, N., Scholz, J., Aytar, Y.: Lossless adaptation of pretrained vision models for robotic manipulation. In: ICLR (2023) [4](#)
79. Silwal, S., Yadav, K., Wu, T., Vakil, J., Majumdar, A., Arnaud, S., Chen, C., Berges, V.P., Batra, D., Rajeswaran, A., et al.: What do we learn from a large-scale study of pre-trained visual representations in sim and real environments? arXiv preprint arXiv:2310.02219 (2023) [4](#), [14](#)
80. Srivastava, N., Mansimov, E., Salakhudinov, R.: Unsupervised learning of video representations using lstms. In: ICML. pp. 843–852. PMLR (2015) [4](#)
81. Stone, A., Xiao, T., Lu, Y., Gopalakrishnan, K., Lee, K.H., Vuong, Q., Wohlhart, P., Zitkovich, B., Xia, F., Finn, C., et al.: Open-world object manipulation using pre-trained vision-language models. In: CoRL (2023) [5](#)
82. Sun, Y., Ma, S., Madaan, R., Bonatti, R., Huang, F., Kapoor, A.: Smart: Self-supervised multi-task pretraining with control transformers. In: ICLR (2023) [4](#)
83. Tassa, Y., Doron, Y., Muldal, A., Erez, T., Li, Y., Casas, D.d.L., Budden, D., Abdolmaleki, A., Merel, J., Lefrancq, A., et al.: Deepmind control suite. arXiv preprint arXiv:1801.00690 (2018) [9](#), [15](#)
84. Team, O.M., Ghosh, D., Walke, H., Pertsch, K., Black, K., Mees, O., Dasari, S., Hejna, J., Xu, C., Luo, J., et al.: Octo: An open-source generalist robot policy (2023) [5](#)
85. Thomas, G., Cheng, C.A., Loynd, R., Frujeri, F.V., Vineet, V., Jalobeanu, M., Kolobov, A.: Plex: Making the most of the available data for robotic manipulation pretraining. In: CoRL. pp. 2624–2641. PMLR (2023) [4](#)
86. Tong, Z., Song, Y., Wang, J., Wang, L.: Videomae: Masked autoencoders are data-efficient learners for self-supervised video pre-training. NeurIPS **35**, 10078–10093 (2022) [3](#), [4](#)
87. Touvron, H., Cord, M., Douze, M., Massa, F., Sablayrolles, A., Jégou, H.: Training data-efficient image transformers & distillation through attention. In: ICLR. pp. 10347–10357. PMLR (2021) [3](#)
88. Van Essen, D.C., Gallant, J.L.: Neural mechanisms of form and motion processing in the primate visual system. Neuron **13**(1), 1–10 (1994) [2](#)
89. Vaswani, A., Shazeer, N., Parmar, N., Uszkoreit, J., Jones, L., Gomez, A.N., Kaiser, Ł., Polosukhin, I.: Attention is all you need. NeurIPS **30** (2017) [7](#)
90. Walke, H.R., Black, K., Zhao, T.Z., Vuong, Q., Zheng, C., Hansen-Estruch, P., He, A.W., Myers, V., Kim, M.J., Du, M., et al.: Bridgedata v2: A dataset for robot learning at scale. In: Conference on Robot Learning. pp. 1723–1736. PMLR (2023) [5](#)
91. Wang, C., Fan, L., Sun, J., Zhang, R., Fei-Fei, L., Xu, D., Zhu, Y., Anandkumar, A.: Mimicplay: Long-horizon imitation learning by watching human play. arXiv preprint arXiv:2302.12422 (2023) [4](#)
92. Wang, J., Dasari, S., Srirama, M.K., Tulsiani, S., Gupta, A.: Manipulate by seeing: Creating manipulation controllers from pre-trained representations. In: ICCV. pp. 3859–3868 (2023) [4](#)
93. Wang, L., Huang, B., Zhao, Z., Tong, Z., He, Y., Wang, Y., Wang, Y., Qiao, Y.: Videomae v2: Scaling video masked autoencoders with dual masking. In: CVPR. pp. 14549–14560 (2023) [2](#), [3](#), [4](#)
94. Wang, L., Zhao, J., Du, Y., Adelson, E.H., Tedrake, R.: Poco: Policy composition from and for heterogeneous robot learning. arXiv preprint arXiv:2402.02511 (2024) [5](#)

95. Wei, C., Fan, H., Xie, S., Wu, C.Y., Yuille, A., Feichtenhofer, C.: Masked feature prediction for self-supervised visual pre-training. In: CVPR. pp. 14668–14678 (2022) [4](#)
96. Whitney, W.F., Agarwal, R., Cho, K., Gupta, A.: Dynamics-aware embeddings. In: ICLR (2020) [4](#)
97. Wu, H., Jing, Y., Cheang, C., Chen, G., Xu, J., Li, X., Liu, M., Li, H., Kong, T.: Unleashing large-scale video generative pre-training for visual robot manipulation. arXiv preprint arXiv:2312.13139 (2023) [4](#)
98. Wuthrich, M., Widmaier, F., Grimminger, F., Joshi, S., Agrawal, V., Hammoud, B., Khadiv, M., Bogdanovic, M., Berenz, V., Viereck, J., et al.: Trifinger: An open-source robot for learning dexterity. In: CoRL. pp. 1871–1882. PMLR (2021) [9](#), [15](#)
99. Xiao, T., Radosavovic, I., Darrell, T., Malik, J.: Masked visual pre-training for motor control. arXiv preprint arXiv:2203.06173 (2022) [2](#), [3](#), [4](#)
100. Xie, Z., Zhang, Z., Cao, Y., Lin, Y., Bao, J., Yao, Z., Dai, Q., Hu, H.: Simmim: A simple framework for masked image modeling. In: CVPR. pp. 9653–9663 (2022) [4](#)
101. Xu, M., Xu, Z., Chi, C., Veloso, M., Song, S.: Xskill: Cross embodiment skill discovery. In: CoRL (2023) [4](#)
102. Yang, J., Guo, S., Wu, G., Wang, L.: Comae: Single model hybrid pre-training on small-scale rgb-d datasets. arXiv preprint arXiv:2302.06148 (2023) [3](#), [13](#)
103. Yang, J., Tan, W., Jin, C., Liu, B., Fu, J., Song, R., Wang, L.: Pave the way to grasp anything: Transferring foundation models for universal pick-place robots. arXiv preprint arXiv:2306.05716 (2023) [5](#)
104. Yu, T., Quillen, D., He, Z., Julian, R., Hausman, K., Finn, C., Levine, S.: Meta-world: A benchmark and evaluation for multi-task and meta reinforcement learning. In: CoRL. pp. 1094–1100. PMLR (2020) [9](#), [15](#)
105. Yuan, C., Wen, C., Zhang, T., Gao, Y.: General flow as foundation affordance for scalable robot learning. arXiv preprint arXiv:2401.11439 (2024) [4](#)
106. Zhou, J., Wei, C., Wang, H., Shen, W., Xie, C., Yuille, A., Kong, T.: ibot: Image bert pre-training with online tokenizer. arXiv preprint arXiv:2111.07832 (2021) [4](#)
107. Zhu, H., Wang, Y., Huang, D., Ye, W., Ouyang, W., He, T.: Point cloud matters: Rethinking the impact of different observation spaces on robot learning. arXiv preprint arXiv:2402.02500 (2024) [4](#)